The Sinking of Warm-Core Rings

RICK CHAPMAN AND DORON NOF

Department of Oceanography, Florida State University, Tallahassee, Florida 32306

(Manuscript received 17 April 1987, in final form 26 October 1987)

ABSTRACT

Intense cooling of a warm-core ring or warming of the fluids surrounding a ring can increase the density of that ring relative to the surrounding fluids. This increase in density can cause the ring to sink under the surrounding fluids. A simple model of this process in a two and one-half layer (two active and one passive layer) ocean consisting of an inviscid Boussinesq fluid on an f-plane is presented. The model assumes that the cooling or heating occurs in such a way as to maintain a uniform density throughout each of the active layers. This special form of the heat flux allows the results for various relative ring densities to be connected through the conservation of potential vorticity. Analytic solutions are constructed and their structure helps to establish the physical processes accompanying the sinking of a ring.

Results show that warm-core rings can sink in a matter of weeks when exposed to typical cold-air outbreaks of -1000 W m^{-2} surface heat flux. The model predicts that when the ring sinks it is overwashed completely, but this overwashing layer is very thin near the center of the ring. It is suggested that the convective mixing associated with continued cooling will act to suppress any surface signature of the overwashing. Applying the same model to the process of differential warming of the surrounding layer, leads to similar results, except that any surface signatures of overwashing will be visible due to the lack of convective mixing. The main difference between cooling the ring and warming the environmental fluid is that, in the former case, the model breaks down when the ring is capped whereas, in the latter case, the ring continues to sink as the warming continues. It is proposed that the above mechanism can lead to the formation of streamers when one portion of the overwashing fluid has been passively marked with a visible tracer such as temperature or chlorophyll.

It is shown that the fluid that initially overwashes the ring originates under the ring, and not from outside the ring. When the ring sinks, this fluid is pushed out to the edge of the ring and spun up in the process. The theory further provides a mechanism for the entrainment of shelf-water organisms that are observed in warm-core rings.

1. Introduction

a. Background

Warm-core rings are highly energetic structures that occur in most of the world's oceans. The structure and dynamics of warm-core rings have been studied for a number of years. Still, there are certain observations for which no satisfactory explanation has been developed. For example, thin cold-water intrusions, called streamers, have often been observed from satellite photographs to spiral in towards the center of warm-core rings (Fig. 1). The dynamics of these streamers have yet to be explained. Also, the surface temperature signature of rings have been observed to disappear for several days after the passage of a cold air outbreak (Shay and Gregg, 1986). Again, the dynamics of such an event have not been explained.

The cooling of warm-core rings has been examined by a number of researchers from differing perspectives. Within recent years an extensive set of measurements in and around several warm-core rings have been made. Measurements were made in ring 82B (the second ring formed during 1982) over an interval of five months in an effort to understand its temporal evolution. Papers by Evans et al. (1985), Joyce and Stalcup (1985), Olson et al. (1985), and Schmitt and Olson (1985) represent the results of these measurements. Each of these analyses was restricted to either simple chronological descriptions of the changes observed in rings, or one-dimensional models of the convective processes responsible for the gross ring changes observed. Schmitt and Olson (1985) did show that lateral entrainment of shelf water was required to explain the changes observed in ring 82B, but offered no detailed explanation of how that entrainment might occur.

Later attempts to model ring evolution have been more sophisticated. Olson (1986) further examined the lateral entrainment required in 82B. His analysis of the salinity changes in the upper 50 m of the ring suggested some combination of an advective radial inflow of fresh surrounding fluid and horizontal diffusivity. Olson states, "The dynamics behind such an inward surface flow, however, are not obvious since this de-

Corresponding author address: Dr. Rick Chapman, Johns Hopkins University, Applied Physics Laboratory, Johns Hopkins Road, Laurel, MD 20707.

FIG. 1. Infrared satellite image of warm-core ring 82B taken on May 18, 1982. In this image the darker shades are cooler. The image is approximately 500 km on each side. A cool streamer of shelf water can be seen wrapping around and into the warmer ring. (Image provided by D. Olson, RSMAS/MPO University of Miami.)

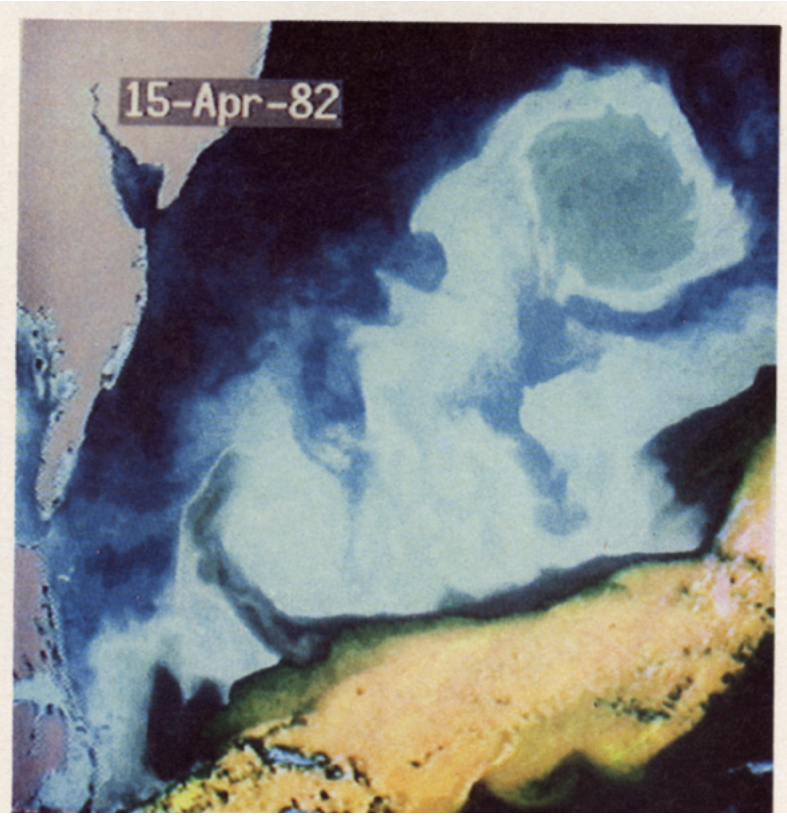

FIG. 14. Infrared satellite image of ring 82B during mid-April. Note the irregular ring edge which displays a series of anticyclonic shelf-water intrusions coming from all directions about the ring. This is consistent with the models prediction of spiral overflooding occurring from all directions as the ring submerges (although it is clearly not proof of such a process). Active streamers would not be observed to penetrate into ring center in such a case due to the mixing associated with convective overturning within the ring. (Image provided by D. Olson, RSMAS/MPO University of Miami.)

mands flow up the pressure gradient." Olson's calculations show that a purely diffusive mechanism for the influx would lead to an *e*-folding time for the surface salinity anomaly in the ring of just 84 days, but such fast processes have not been observed. Olson then states that shear dispersion, as described by Dewar and Flierl (1985), could reduce the required lateral diffusivity by increasing the diffusive flux. Flierl and Mied (1985) examined the effects of secondary circulation in a frictionally-decaying warm-core ring. Their results can account for the observed mixed-layer shallowing within a ring (assuming an unusually large vertical mixing coefficient of 100 m^2 s^{-1}), but they do not generate sufficiently fast radial velocities to explain streamers.

All of the previously mentioned studies were of surfaced warm-core rings. The structure of submerged rings has been described by Ikeda (1982) using a numerical model. Gill (1981) described the form of a homogeneous submerged ring that was injected into a uniformly-stratified, infinitely-deep ocean. For other aspects of ring dynamics, the reader is referred to the Warm-Core Rings Collection appearing in the *Journal of Geophysical Research* (Vol. 90, No. C5, 1985) and the Warm-Core Ring issue of Deep-Sea Research (Vol. 33, Nos. 11/12, 1986). These two special issues contain numerous articles on the physics, chemistry, and biology of warm-core rings.

The present research is an attempt to link together the observations by examining the dynamics of a warm-core ring that becomes denser than the surrounding fluid. The conjecture is that a cold-air outbreak could cool a warm-core ring to the point where it would sink and be overwashed by the surrounding fluid. Alternatively, differential vernal warming of the fluids surrounding a warm-core ring could cause those fluids to become less dense than the ring, again leading to the overwashing of the ring. It is further speculated that, in some cases, this sinking can lead to the formation of streamers through the spiral inward flow of a passive tracer (e.g., heat or chlorophyll) in the overwashing fluid. In order to simplify the discussion, the model is presented in terms of the effects of ring cooling. A discussion of the alternative of differential warming appears towards the end of the paper.

b. *Model overview*

The model in the study consists of three layers under a rigid lid: a shallow upper layer (hereafter referred to as the mixed layer), an infinitely deep bottom layer, and a zero-potential vorticity layer which comprises the ring itself (Fig. 2). The fluid is assumed to be Boussinesq and the flow to be hydrostatic. As in Gill (1981), the ring is modeled as if it were formed through an injection of fluid into a resting two-layer system. The ring starts out lighter (but more saline) than the shallow mixed layer but then is cooled to become heavier than the mixed layer. Note that this cooling *need not be to a temperature below* that of the mixed-layer since warm-core rings are considerably more saline than the mixed-layer.

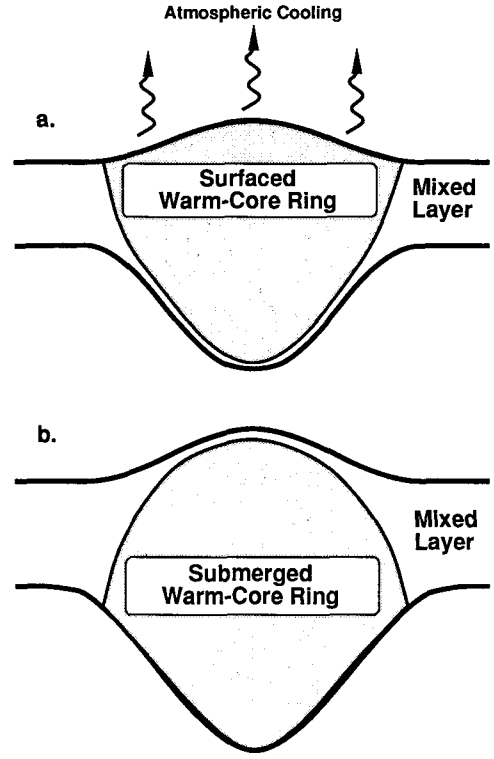

FIG. 2. Conceptual drawing of a warm-core ring (a) before and (b) after the ring has (due to differential atmospheric cooling) sunk below the surrounding mixed layer.

The process of the ring cooling and sinking is shown schematically in Figs. 2a and 2b. The interfaces in Fig. 2a show the ring to be initially above the mixed layer. At a later time, after some cooling has occurred, the ring will sink below the mixed layer and appear as shown in Fig. 2b. It will be shown analytically that when the ring is cooled below the density of the surrounding mixed layer, it sinks *completely below the upper layer;* partial sinking cannot occur. The mixed-layer fluid, which was originally below the ring when the ring was first formed, is initially displaced to the outer edge of the ring as the ring sinks below the surface. The mixed-layer fluid then overfloods the ring as the ring continues to be cooled. The model concentrates on the flow in the mixed layer during this cooling and sinking process.

Following Nof (1983) and Adamec and Elsberry (1985), the cooling is assumed to be tapered in such a way as to increase the density of the ring uniformly throughout its entire lifetime. This special form of the cooling, shown schematically in Fig. 3a, and discussed in detail in the following section, allows the results for various ring densities to be connected through the conservation of potential vorticity. The cooling is further

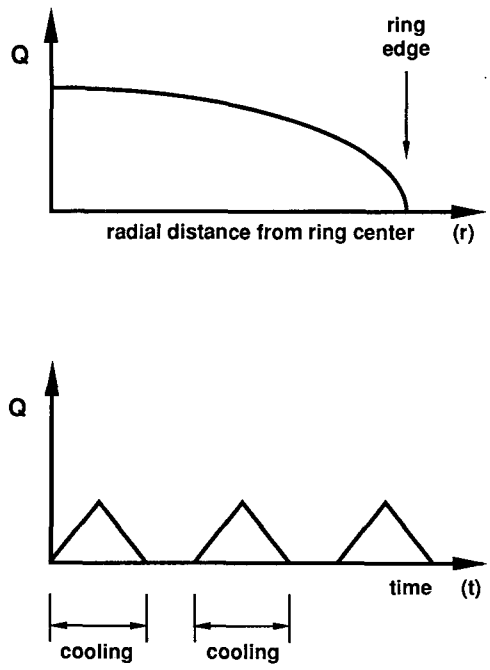

FIG. 3. Conceptual drawing of the heat flux (Q) used in the model. The top panel, a plot of heat flux vs radial distance from ring center, shows how the heat flux is tapered over the ring in order to maintain a uniform ring density. The detailed dependence of Q on r is discussed in section 2a. The lower panel, plotting heat flux vs time, shows the periodic cooling structure used in the model. The time scale associated with these cooling events is on the order of days.

assumed to be intermittent. That is, each cooling period is followed by a period of at least one day where there is no heat flux (Fig. 3b). Note that the intermittent cooling episodes shown in Fig. 3b correspond to a finite cooling time, but instantaneous cooling episodes of the kind considered by Stommel and Veronis (1980) are also applicable to our model. The intermittent nature of the cooling permits any inertial–gravity waves generated during the process of cyclo-geostrophic adjustment to propagate away. Thus the model can be solved analytically in terms of a steady-state solution at each ring density. All flows are assumed to be steady (at least at times scales short with respect to the cooling) and axisymmetric. (It is believed that these adjustment waves are small if the cooling is slow enough, but a proof of this conjecture is beyond the scope of this analysis. In support of this conjecture, the analysis of Veronis, 1956, suggests that adjustment waves of this type are small if the forcing occurs over more than one-half of a pendulum day, here about 17 h.)

The model is divided into two sets of equations, one representing the case of a surfaced ring and one representing the case of a submerged ring. In both cases, the ring is assumed to have zero-potential vorticity throughout. This assumption is a convenient one that has been used in a number of previous studies (e.g., Nof, 1981; Killworth, 1983). The mixed layer is assumed to have a uniform potential vorticity of f/H, corresponding to an initially resting layer of depth H. As previously mentioned, the model assumes that the ring was formed through the injection of the ring material at a point on top of the previously resting mixed layer. This formation process is consistent with the above assumptions. Although other formation processes can be envisioned, it is argued in section 6 that this particular formation process is the most appropriate one to consider.

The remainder of this paper is organized as follows. The next section discusses the formulation; sections 3 and 4 describe in detail the models and section 5 presents the results of the study with plots of ring interfaces, velocities and fluid parcel trajectories. In the final section the results are summarized and the limitations and implications of the study are discussed.

2. Formulation

a. Fundamental equations

Consider the flow of an inviscid fluid in a shallow upper layer on an f-plane. The origin of the cylindrical coordinate system is located at the bottom of the layer with undisturbed depth H and the system rotates uniformly about the vertical axis (see Fig. 4). Assuming that the flow is hydrostatic and the fluid is Boussinesq, the governing equations are

$$\frac{\partial V_r}{\partial t} + V_r\frac{\partial V_r}{\partial r} + \frac{V_\theta}{r}\frac{\partial V_r}{\partial \theta} - \frac{V_\theta^2}{r} - fV_\theta = -\rho_0^{-1}\frac{\partial p}{\partial r} \tag{2.1a}$$

$$\frac{\partial V_\theta}{\partial t} + V_r\frac{\partial V_\theta}{\partial r} + \frac{V_\theta}{r}\frac{\partial V_\theta}{\partial \theta} + \frac{V_rV_\theta}{r} + fV_r = -\rho_0^{-1}r^{-1}\frac{\partial p}{\partial \theta} \tag{2.1b}$$

$$\frac{\partial p}{\partial z} = -\rho g \tag{2.1c}$$

$$\frac{1}{r}\frac{\partial}{\partial r}(rV_rh) + \frac{1}{r}\frac{\partial}{\partial \theta}(V_\theta h) = 0 \tag{2.1d}$$

$$\frac{\partial \rho}{\partial t} + V_r\frac{\partial \rho}{\partial r} + \frac{V_\theta}{r}\frac{\partial \rho}{\partial \theta} + \frac{V_r\rho}{r} = -\frac{\alpha_T}{c_p}\frac{\partial F}{\partial z}. \tag{2.1e}$$

In these equations, V_r and V_θ are radial and azimuthal velocities, t is time, f the Coriolis parameter, ρ the density, ρ_0 the mean density, p the pressure, g the gravitational acceleration, h the depth of the layer, α_T the thermal expansion coefficient for the fluid, c_p the specific heat of the fluid, and F is the heat flux density.

It is now assumed that the layer is well mixed so that its density is depth independent. This is a reasonable assumption since convection will act quickly to mix the effects of surface cooling vertically throughout

the layer. Further assume that there is no heat flux through the sides or bottom of the layer. Then (2.1e) can be integrated vertically from the bottom of the layer at depth h to the free surface to obtain

$$\frac{\partial \rho}{\partial t} + V_r \frac{\partial \rho}{\partial r} + \frac{V_\theta}{r}\frac{\partial \rho}{\partial \theta} + \frac{V_r \rho}{r} = -\frac{\alpha_T}{h c_p} Q \qquad (2.2)$$

where Q is the heat flux through the top of the ring. From (2.2) and the assumption that the density is *initially* uniform throughout the layer, it can be seen that a spatially homogeneous density can be maintained if the heat flux Q is proportional to the layer depth, h. Under these assumptions it can be shown (Chapman, 1987) that the potential vorticity of the fluid layer $[(\partial V_\theta/\partial r + V_\theta/r - (1/r)\partial V_r/\partial \theta + f)/h]$ is conserved.

The key assumption here is that the heat flux applied to the ring is tapered in such a way as to maintain a uniform density throughout the ring (Fig. 3, top panel). If this assumption is not made, then the potential vorticity will no longer be conserved and a different form of analysis would be required. Although it is doubtful that this exact type of cooling event would occur in nature, it is believed that the results of the model retain many of the dynamic characteristics of more realistic cooling events (e.g., see the discussion by Nof, 1983). Dewar (1987), on the other hand, has investigated the flows resulting from the uniform surface cooling of a warm-core ring. Dewar's study suggests that the uniform cooling of a ring causes an inward surface flow and outward deep flow within the ring.

Under the Boussinesq approximation the physical forcing associated with cooling enters into the momentum equations through the hydrostatic equation. Combining the results of integrating (2.1c) over depth and (2.2) over time yields:

$$p = -\left(1 - \frac{\alpha_T}{h\rho_0 c_p} Qt\right)\rho_0 g(H + \eta - z) \qquad (2.4),$$

where η is the free surface displacement and H is the upper layer undisturbed depth. Substituting (2.4) into the horizontal momentum equations (2.1a) and (2.1b),

$$\frac{\partial V_r}{\partial t} + V_r \frac{\partial V_r}{\partial r} + \frac{V_\theta}{r}\frac{\partial V_r}{\partial \theta} - \frac{V_\theta^2}{r} - f V_\theta = \left(1 - \frac{\alpha_T}{h\rho_0 c_p} Qt\right) g \frac{\partial \eta}{\partial r} \qquad (2.5a)$$

$$\frac{\partial V_\theta}{\partial t} + V_r \frac{\partial V_\theta}{\partial r} + \frac{V_\theta}{r}\frac{\partial V_\theta}{\partial \theta} + \frac{V_r V_\theta}{r} + f V_r = \left(1 - \frac{\alpha_T}{h\rho_0 c_p} Qt\right) g r^{-1} \frac{\partial \eta}{\partial \theta} \qquad (2.5b)$$

show how the horizontal momentum equations are forced by surface cooling.

b. Boundary conditions

The model consists of the previously derived momentum and conservation equations applied to the multi-layer geometry of an axisymmetric sinking ring together with an appropriate set of boundary conditions. The boundary conditions related to the form of the heat flux at the surface of the ring and the assumption of no heat flux through the ring walls have already been described. The additional necessary boundary conditions are discussed below.

The first two additional boundary conditions are

$$V_\theta(r) = 0; \quad r = 0 \qquad (2.6a)$$

$$V_\theta(r) = 0; \quad r \to \infty \qquad (2.6b)$$

which state that all azimuthal velocities within the model are zero at the ring center and at infinity. The restriction at ring center ($V_\theta \to 0$ as $r \to 0$) eliminates singular solutions for the velocity, whereas the restriction at infinity is due to the assumption that any effects of localized forcing will stay localized.

Two additional constraints placed on the system are the continuity of pressure and velocity within each layer. At the edge of the ring (at radius r_0), these conditions take on the form:

$$p^-(z) = p^+(z); \quad r = r_0, \qquad (2.7a)$$

$$V_\theta^-(z) = V_\theta^+(z); \quad r = r_0, \qquad (2.7b)$$

where the minus superscript indicates the value evaluated just inside the ring edge, the plus superscript denotes evaluation outside of the ring edge. The continuity of velocity arises from the conservation of angular momentum ($rV_\theta + fr^2/2$). The basic argument states that since the fluid is hydrostatic, all fluid parcels within a layer move as columns. Furthermore, the axisymmetry of the system forces parcel motion to be restricted to concentric cylinders of fluid. Two thin, concentric cylinders which are initially adjacent will remain adjacent throughout the process of adjustment forced by the cooling. Prior to the initial ring injection, the angular momentum is a continuous function of radius ($=fr^2/2$) and during the adjustment process the parcels retain their angular momentum. Therefore, the angular momentum remains continuous during the adjustment process and so the velocity must also be continuous. Both of these constraints appear later as boundary conditions in the matching of separate solutions obtained for the regions adjacent to the ring and outside of the ring.

The final boundary condition is the geometrical constraint that the height of the ring, h_R, goes to zero at some distance from ring center, r_0. This constraint, expressed by,

$$h_R(r) = 0; \quad r = r_0 \qquad (2.8)$$

is required by (2.5a) and (2.5b) as shown by Flierl (1979). Here the subscript R indicates that the variable is associated with the ring.

3. Surfaced ring model

a. Governing equations

The model is based on the momentum and potential vorticity equations for the axisymmetric flow of a surfaced ring in an otherwise two-layer ocean. In our cylindrical coordinate system r is the radial coordinate, η the free surface displacement, ξ_{Rl} the displacement of the lower surface of the ring (as measured from the level of the undisturbed mixed-layer interface), ρ the mixed layer density, $\rho + \Delta\rho_R$ the ring density (here $\Delta\rho_R < 0$), $\rho + \Delta\rho_D$ the lower layer density, $V_{\theta M}$ is the azimuthal velocity in the mixed layer, and $V_{\theta R}$ is the azimuthal velocity within the ring. The subscripts R, M, D, l and u are used to indicate the ring, mixed layer, deep lower layer, lower interfaces and upper interfaces, respectively. The lower layer is infinitely deep and essentially passive. The edge of the ring is denoted by r_0 and the possible intersection of the ring-mixed layer interface with the mixed layer-lower layer interface is denoted by r_1. Due to the geometry, the system is naturally divided into three regions,

$$\text{Region I:} \quad r \leq r_1,$$

$$\text{Region II:} \quad r_1 < r \leq r_0,$$

$$\text{Region III:} \quad r > r_0,$$

as displayed in the top view in Fig. 4.

The equations that govern this system in the three different regions are

Region I:

$$\frac{V_{\theta R}^2}{r} + f V_{\theta R} = g \frac{\partial \eta}{\partial r} \tag{3.1a}$$

$$\xi_{Rl} = \frac{\rho}{\Delta\rho_R - \Delta\rho_M}\eta + \frac{\Delta\rho_R}{\Delta\rho_R - \Delta\rho_M} H \tag{3.1b}$$

$$0 = \frac{V_{\theta R}}{r} + \frac{\partial V_{\theta R}}{\partial r} + f \tag{3.1c}$$

$$\xi_{Rl} = \xi_M \tag{3.1d}$$

Region II:

$$\frac{V_{\theta R}^2}{r} + f V_{\theta R} = g \frac{\partial \eta}{\partial r} \tag{3.2a}$$

$$\frac{V_{\theta M}^2}{r} + f V_{\theta M} = g \frac{\partial \eta}{\partial r} + \frac{\Delta\rho_R}{\rho} g \frac{\partial \xi_{Rl}}{\partial r} \tag{3.2b}$$

$$\eta + \frac{\Delta\rho_R}{\rho}(H + \xi_{Rl}) - \frac{\Delta\rho_D}{\rho}\xi_M = 0 \tag{3.2c}$$

$$\frac{f}{H}(\xi_M - \xi_{Rl}) = \frac{V_{\theta M}}{r} + \frac{\partial V_{\theta M}}{\partial r} + f \tag{3.2d}$$

$$0 = \frac{V_{\theta R}}{r} + \frac{\partial V_{\theta R}}{\partial r} + f \tag{3.2e}$$

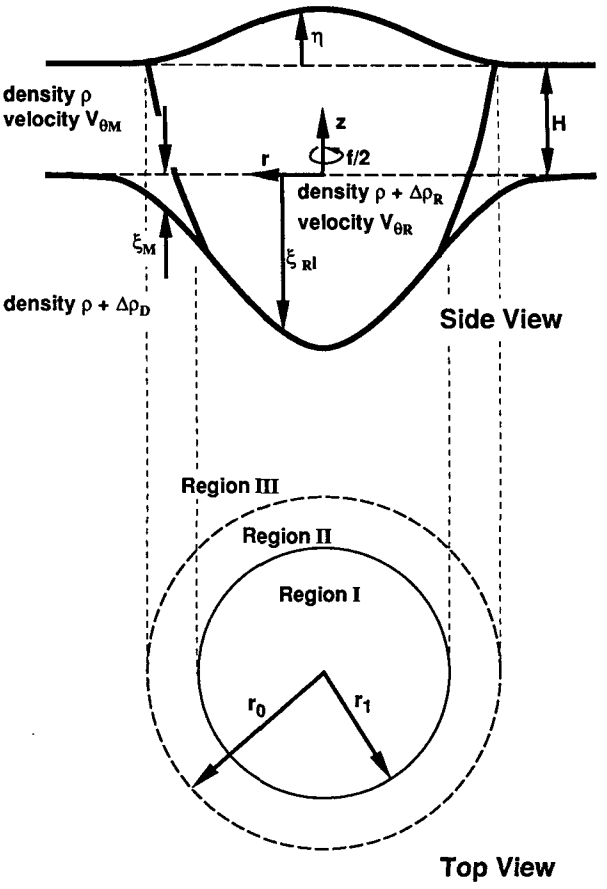

FIG. 4. Schematic diagram of the surfaced ring model. Throughout the model, η is the free surface displacement, ξ the internal surface displacements [measured from the undisturbed mixed layer depth (H)], and V_θ is azimuthal velocity. The subscripts M, R and D indicate the mixed layer, ring and deep layer, respectively. The additional subscripts l and u are used to indicate the lower and upper ring interfaces. The model is naturally divided into three regions: Region I is the two-layer region where $r < r_1$, Region II is the three-layer region outside Region I but inside the ring edge ($r_1 < r < r_0$), and Region III is the region outside of the ring edge ($r > r_0$).

Region III:

$$\frac{V_{\theta M}^2}{r} + f V_{\theta M} = g \frac{\partial \eta}{\partial r} \tag{3.3a}$$

$$\xi_M = \frac{\rho}{\Delta\rho_D}\eta \tag{3.3b}$$

$$\frac{f}{H}(\eta + \xi_M) = \frac{V_{\theta M}}{r} + \frac{\partial V_{\theta M}}{\partial r}. \tag{3.3c}$$

These equations represent the momentum balance in the ring and mixed layer [(3.1a), (3.2a), (3.2b), and (3.3a)], the condition of no flow in the lower layer [(3.1b), (3.2c), and (3.3b)], and the conservation of potential vorticity in the ring and mixed layers [(3.1c), (3.2d), (3.2e), and (3.3c)]. Equation (3.1d) is the geometric condition for the intersection of the ring-mixed

layer interface and the mixed layer-lower layer interface for Region I.

Before proceeding, the method of development of these equations and their solution is outlined. First, some simplifications will be made to these equations by solving for the velocity within the ring and then substituting this velocity into the remaining equations. A set of scalings are introduced to nondimensionalize the remaining equations. The equations can then be combined to form a single velocity field equation for each of the three regions. It is shown in Appendix A that Region I cannot exist, so the problem is further simplified by only considering Regions II and III. The solution for the velocity in the mixed layer under the ring (Region II) will be in terms of a power series. A perturbation expansion in small Rossby number will be used to solve the field equation outside the ring (Region III). The two solutions will then be combined using appropriate matching conditions.

We begin by solving the potential vorticity equation for the ring, which immediately yields $V_{\theta R} = -fr/2$. Then, the rigid-lid approximation is applied (to eliminate η from the potential vorticity equation in Region III) and the following scalings are introduced:

$$r = R_d\hat{r}, \quad \text{where} \quad R_d^2 \equiv \frac{gH}{f^2}\frac{\Delta\rho_D}{\rho}$$

$$\eta = H\frac{\Delta\rho_D}{\rho}\hat{\eta}$$

$$\xi_i = H\hat{\xi}_i$$

$$V_{\theta i} = fR_d\hat{V}_{\theta i} \tag{3.4},$$

where R_d is the internal radius of deformation *outside* the ring and the carats indicate the nondimensional parameters. Finally, the nondimensional ratio of the density defects can be defined as $d = \Delta\rho_R/\Delta\rho_D$. Dropping the carats, the nondimensionalized governing equations then become

Region I:

$$\frac{\partial\eta}{\partial r} = -\frac{r}{4} \tag{3.5a}$$

$$\xi_{RI} = \frac{1}{1-d}(\eta + 1) \tag{3.5b}$$

$$\xi_{RI} = \xi_M \tag{3.5c}$$

Region II:

$$\frac{\partial\eta}{\partial r} = -\frac{r}{4} \tag{3.6a}$$

$$\frac{V_{\theta M}^2}{r} + V_{\theta M} = \frac{\partial\eta}{\partial r} + d\frac{\partial\xi_{RI}}{\partial r} \tag{3.6b}$$

$$\eta + d(1 + \xi_{RI}) - \xi_M = 0 \tag{3.6c}$$

$$\xi_M - \xi_{RI} = \frac{V_{\theta M}}{r} + \frac{\partial V_{\theta M}}{\partial r} + 1 \tag{3.6d}$$

Region III:

$$\frac{V_{\theta M}^2}{r} + V_{\theta M} = \frac{\partial\eta}{\partial r} \tag{3.7a}$$

$$\xi_M = \eta \tag{3.7b}$$

$$\xi_M = \frac{V_{\theta M}}{r} + \frac{\partial V_{\theta M}}{\partial r}. \tag{3.7c}$$

From (3.6a)–(3.6d) the velocity field equation for the flow in the mixed layer below the ring (Region II) can be derived,

$$r^2\frac{\partial^2 V_{\theta M}}{\partial r^2} + r\frac{\partial V_{\theta M}}{\partial r} - V_{\theta M} + \frac{1-d}{d}(rV_{\theta M}^2 + r^2V_{\theta M}) + \frac{r^3}{4d} = 0. \tag{3.8}$$

In addition, within Region II, η, ξ_M and ξ_{RI} can be expressed in terms of the velocity and its derivative,

$$\eta = c - \frac{r^2}{8} \tag{3.9a}$$

$$\xi_M = (1-d)^{-1}\left[c - \frac{r^2}{8} - d\left(\frac{V_{\theta M}}{r} + \frac{\partial V_{\theta M}}{\partial r}\right)\right] \tag{3.9b}$$

$$\xi_{RI} = (1-d)^{-1}\left[c + d - 1 - \frac{r^2}{8} - \left(\frac{V_{\theta M}}{r} + \frac{\partial V_{\theta M}}{\partial r}\right)\right] \tag{3.9c}$$

where c is a constant of integration. For convenience, one additional level of simplification of (3.8) and (3.9) can be obtained by transforming from r and $V_{\theta M}$ to α and ϑ_M according to

$$V_{\theta M} = -\frac{d}{r_0(1-d)}\vartheta_M - \frac{r_0\alpha}{2} \quad \text{and} \quad r = r_0\alpha \tag{3.10}$$

where, as before, r_0 is the radius of the ring. Substitution of (3.10) into (3.8) and (3.9) yields

$$\alpha^2\frac{\partial^2\vartheta_M}{\partial\alpha^2} + \alpha\frac{\partial\vartheta_M}{\partial\alpha} - \vartheta_M - \alpha\vartheta_M^2 = \frac{(1-d)r_0^4\alpha^3}{4d} \tag{3.11a}$$

$$\eta = c - \frac{r_0^2\alpha^2}{8} \tag{3.11b}$$

$$\xi_M = (1-d)^{-1}\left[c + d - \frac{r_0^2\alpha^2}{8} + \frac{d^2}{r_0^2(1-d)}\left(\frac{\vartheta_M}{\alpha} + \frac{\partial\vartheta_M}{\partial\alpha}\right)\right] \tag{3.11c}$$

$$\xi_{RI} = (1-d)^{-1}\left[c + d - \frac{r_0^2\alpha^2}{8} + \frac{d}{r_0^2(1-d)}\left(\frac{\vartheta_M}{\alpha} + \frac{\partial\vartheta_M}{\partial\alpha}\right)\right]. \tag{3.11d}$$

Equations (3.11a)–(3.11d), with appropriate boundary conditions, completely describe the flow in the 3-layer region of the system, Region II.

As previously mentioned, it can be shown that in fact there can be no Region I (appendix A) and, hence, no intersection between the ring-mixed layer interface and the mixed layer-lower layer interface. The system of equations is thus further simplified by only considering the solutions within Region II and Region III.

b. Solution in Region II

Equation (3.11a) can be solved analytically using a regular power series. Substitution of the form

$$\vartheta_M = \sum_{i=1}^{\infty} a_i \alpha^i \tag{3.12}$$

yields the recursion relations:

$$a_2 = 0$$

$$a_3 = a_1^2 + \frac{(1-d)r_0^4}{4d}$$

$$a_m = \frac{2}{(m^2-1)} \begin{cases} 0, & m \text{ even} \\ \sum_{i=1}^{(m-1)/2} a_i a_{m-i-1}, & m \text{ odd.} \end{cases} \tag{3.13}$$

This solution needs to be matched to a solution of the simpler two-layer system that occurs just outside the edges of the ring.

c. Solution outside the ring (Region III)

The momentum and potential vorticity equations for Region III, (3.7a)–(3.7c), can be combined to obtain the velocity field equation,

$$r^2 \frac{\partial^2 V_{\theta M}}{\partial r^2} + r \frac{\partial V_{\theta M}}{\partial r} - (1+r^2)V_{\theta M} - rV_{\theta M}^2 = 0 \tag{3.14}$$

where $r \in [r_0, \infty]$ and $V_{\theta M}(\infty) = 0$. Again, the field equation can be simplified through the choice of a suitable transformation. Here, let $\vartheta = V_{\theta M}/r_0$ to obtain

$$r^2 \frac{\partial^2 \vartheta}{\partial r^2} + r \frac{\partial \vartheta}{\partial r} - (1+r^2)\vartheta - rr_0\vartheta^2 = 0. \tag{3.15}$$

Now assuming $\vartheta(r_0) = \epsilon$ (implying that the velocities in the mixed-layer are small compared to the orbital speed within the ring), (3.15) can be linearized by expanding in ϵ,

$$\vartheta = \epsilon\vartheta_1 + \epsilon^2\vartheta_2 + \epsilon^3\vartheta_3 + \cdots. \tag{3.16}$$

This expansion is equivalent to expanding for small Rossby number, since $\epsilon = f V_{\theta M}(r_0)(fr_0)^{-1}$. Hence, in contrast to the interior which is highly nonlinear, the exterior is quasi-geostrophic. We shall see that this approach is valid as long as the density defect ratio (d) is not too close to zero.

To lowest order, (3.15) becomes

$$r^2 \frac{\partial^2 \vartheta_1}{\partial r^2} + r \frac{\partial \vartheta_1}{\partial r} - (1+r^2)\vartheta_1 = 0 \tag{3.17}$$

with the boundary conditions $\vartheta_1(r_0) = 1$ and $\vartheta_1(\infty) = 0$ [see (2.5a) and (2.5b)]. The solution of (3.17) is

$$\vartheta_1 = aK_1(r) = a_0 e^{-r}\left(r^{-1/2} + \frac{3}{8}r^{-3/2}\right) + \cdots + O(e^{-r}r^{-5/2}) \quad \text{where} \quad a_0 = e^{r_0}\left(r_0^{-1/2} + \frac{3}{8}r_0^{-3/2}\right)^{-1} \tag{3.18}$$

and K_1 is the modified Bessel function of the first kind. The two-term asymptotic expansion for K_1 is used in the model since the second-order equation below involves terms of ϑ_1^2. The error in this asymptotic representation is less than 3% for all $r > 2$. Since we only consider rings with radii larger than five, this restriction on the ring size does not present a problem.

The second-order problem is

$$r^2 \frac{\partial^2 \vartheta_2}{\partial r^2} + r \frac{\partial \vartheta_2}{\partial r} - (1+r^2)\vartheta_2 = r_0 r \vartheta_1^2 = a_0^2 r_0 e^{-2r}\left(1 + \frac{3}{4}r^{-1}\right) + \cdots + O(e^{-2r}r^{-2}) \tag{3.19}$$

with the boundary conditions $\vartheta_2(r_0) = 0$ and $\vartheta_2(\infty) = 0$. The total asymptotic solution is

$$\vartheta_2 = e^{-2r_0}\left(r_0^{-1/2} + \frac{3}{8}r_0^{-3/2}\right)^{-2}\left[r_0 e^{-2r}\left(\frac{1}{3}r^{-2} - \frac{5}{12}r^{-3}\right) - r_0^{-1/2}e^{-r_0-r}\left(\frac{8r_0-10}{24r_0+9}\right)\left(r^{-1/2} + \frac{3}{8}r^{-3/2}\right)\right] + \cdots + O(e^{-2r}r^{-2}) \tag{3.20}$$

In this solution, the error resulting from the termination of the asymptotic expansion to two-terms is estimated to be less than 6% for $r > 4$.

Combining these solutions yields an analytic expression for the velocity field in the mixed layer outside the ring,

$$V_{\theta M} = V_{\theta M}(r_0)e^{r_0-r}\left(r_0^{-1/2} + \frac{3}{8}r_0^{-3/2}\right)^{-1}\left(r^{-1/2} + \frac{3}{8}r^{-3/2}\right) + V_{\theta M}^2(r_0)\left(r_0^{-1/2} + \frac{3}{8}r_0^{-3/2}\right)^{-2}\left[e^{2r_0-2r}\left(\frac{1}{3}r^{-2} - \frac{5}{12}r^{-3}\right) - r_0^{-3/2}\frac{8r_0-10}{24_{r_0}+9}e^{r_0-r}\left(r^{-1/2} + \frac{3}{8}r^{-3/2}\right)\right] + \cdots + O(\epsilon^3) + O(e^{-2r}r^{-4}). \tag{3.21}$$

Thus, the solution in Region III consists of a small Rossby number perturbation expansion where each of the individual terms in the expansion is itself an

asymptotic expansion. As indicated, the use of a small Rossby number expansion restricts the model to values of the density defect ratio, d, which are different than zero. This can be most easily seen by considering the case where $d = 0$, that is, when the mixed layer density equals the ring density. In this case, the ring-mixed layer interface must be vertical and all of the fluid in the mixed layer has been pushed outside of the ring. This forces the mixed layer parcels adjacent to the ring wall to spin up to a nondimensional velocity of $-r_0/2$. Thus when $d = 0$, the Rossby number just outside the ring wall, ϵ, is not small but of order one. (We have been unable to derive an analytic expression for the flow for the case where d is near or equal to zero.)

d. Matching the solutions

Despite the complexity of the two solutions obtained so far, the solutions under and outside the ring can be matched at the ring edge. As mentioned before, the matching requires that the velocity and the pressure in the mixed layer be continuous at the ring edge, r_0. The former results from angular momentum arguments whereas the latter is a property of all fluids. It is clear that the continuity of the hydrostatic pressure implies that the free surface displacement, η, and the interface displacement, ξ_M, are both continuous. The above conditions, together with potential vorticity conservation [(3.6d) and (3.7c)] and the boundary condition $\xi_{RI}(r_0) = -1$ [derived from (2.7)], imply that the derivative of the velocity is also continuous at r_0. In view of this, it is concluded that the continuity of the velocity and its first derivative, given by

$$V^{II}_{\theta M}(r_0) = V^{III}_{\theta M}(r_0) \tag{3.22}$$

$$\frac{\partial V^{II}_{\theta M}}{\partial r}(r_0) = \frac{\partial V^{III}_{\theta M}}{\partial r}(r_0) \tag{3.23}$$

(where the superscripts denote the region), assures the continuity of pressure.

The problem is now to match the solution in Region II, (3.12) and (3.13), to the solution in Region III, (3.21). At this point it is convenient to introduce the parameter q,

$$q = \frac{(1 - d)r_0^4}{4d} \tag{3.24}$$

which, together with the velocity shear at the center, a_1 [from (3.12)], is sufficient to specify the power series solution for the mixed-layer velocity in Region II [(3.12) and (3.13)]. The parameters q and a_1, together with the velocity at the ring's edge $V^{III}_{\theta M}(r_0)$, the radius of the ring r_0, and the density defect ratio d, provide a set of five variables.

Taking q and a_1 to be given, there are three remaining unknowns $V^{III}_{\theta M}(r_0)$, r_0, and d. These unknowns can be solved for by applying the three algebraic conditions given in (3.22)–(3.24). To do so, $V^{III}_{\theta M}(r_0)$ is eliminated from the condition associated with the continuity of velocity (3.22) and the resulting equation is incorporated into the condition associated with the continuity of shear (3.23). This yields an eighth-order polynomial in r_0 which is solved numerically; only one physically relevant root (i.e., real and nonnegative) is found. With the solution for r_0, the density defect ratio, d, can be computed from (3.24).

The above procedure gives a set of solutions for various d and ring volumes. The desired solutions for a given volume are then selected from this set. The results of this analysis are shown in section 5.

4. Submerged ring model

Submerged rings are modeled in an analogous manner to the surfaced rings, so only the major points and differences are discussed here.

a. Model coordinate system and equations

The coordinate system for the submerged ring case is shown in Fig. 5. It differs from that of the surface

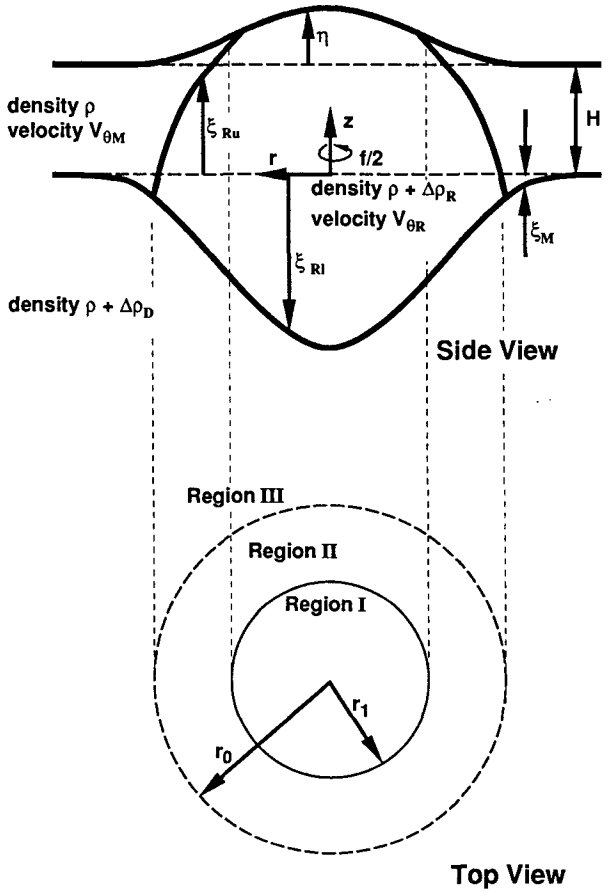

FIG. 5. Schematic diagram of the submerged ring model. The notation is the same as described in the caption of Fig. 4.

ring in the definitions of the interface displacements ξ_{Ru} and ξ_{Rl} within the ring. In this case, ξ_{Ru} is the displacement of the mixed layer-ring interface above the undisturbed mixed layer interface and ξ_{Rl} is the displacement of the lower layer-ring interface below the undisturbed mixed layer interface. Note that since the ring is denser than the mixed layer for the submerged case, $d > 0$. Again, the system is naturally divided into three regions, and, as before, it can be shown that Region I cannot exist and, hence, there can be no intersection of the ring with the free surface (Appendix B).

Applying the same scalings as in (3.4), the nondimensionalized equations governing this system in Regions II and III can be derived to be

Region II:

$$\frac{V_{\theta M}^2}{r} + V_{\theta M} = \frac{\partial \eta}{\partial r} \tag{4.3a}$$

$$\frac{\partial \eta}{\partial r} + d\frac{\partial \xi_{Ru}}{\partial r} + \frac{r}{4} = 0 \tag{4.3b}$$

$$\xi_{Rl} = \frac{1}{1-d}\eta + \frac{d}{1-d}\xi_{Ru} \tag{4.3c}$$

$$\xi_{Ru} = \frac{V_{\theta M}}{r} + \frac{\partial V_{\theta M}}{\partial r} \tag{4.3d}$$

Region III:

$$\frac{V_{\theta M}^2}{r} + V_{\theta M} = \frac{\partial \eta}{\partial r} \tag{4.4a}$$

$$\xi_M = \eta \tag{4.4b}$$

$$\xi_M + \frac{V_{\theta M}}{r} + \frac{\partial V_{\theta M}}{\partial r} = 0. \tag{4.4c}$$

From (4.3) the velocity field equation for Region II can be derived to be

$$r^2\frac{\partial^2 V_{\theta M}}{\partial r^2} + r\frac{\partial V_{\theta M}}{\partial r} - V_{\theta M} - \frac{1}{d}(rV_{\theta M}^2 + r^2 V_{\theta M}) - \frac{r^3}{4d} = 0. \tag{4.5}$$

Again, this field equation can be further simplified by applying the following transformations:

$$V_{\theta M} = \frac{d}{r_0}\vartheta_M - \frac{r_0\alpha}{2} \quad \text{and} \quad r = r_0\alpha, \tag{4.6}$$

resulting in

$$\alpha^2\frac{\partial^2 \vartheta_M}{\partial \alpha^2} + \alpha\frac{\partial \vartheta_M}{\partial \alpha} - \vartheta_M - \alpha\vartheta_M^2 = 0 \tag{4.7}$$

which is the homogeneous form of (3.11a).

b. Solution in Region II

Equation (4.7) is solved by a power series in the same manner as before, yielding the recursion relation:

$$a_2 = 0$$

$$a_3 = a_1^2$$

$$a_m = \frac{2}{(m^2-1)}\begin{cases} 0, & m \text{ even} \\ \sum_{i=1}^{(m-1)/2} a_i a_{m-i-1}, & m \text{ odd.} \end{cases} \tag{4.8}$$

c. Solution in Region III and the matching of solutions

The equations for Region III are identical for the submerged and surfaced cases, so the solution for this region is given by (3.21). The solutions over the ring and outside the ring need to be matched again using the continuity of velocity and its derivative [(3.22) and (3.23)]. In contrast to the surfaced case, the power series solution for the mixed-layer velocity on Region II is determined by a single parameter, a_1. Thus, the submerged model has only four variables at this point: the velocity shear at the center a_1, the velocity at the ring's edge $V_{\theta M}^{III}(r_0)$, the radius of the ring r_0, and d.

Here, take a_1 and r_0 to be given so that there are two unknowns, $V_{\theta M}^{III}(r_0)$ and d. As before, $V_{\theta M}^{III}(r_0)$ is eliminated through the application of the continuity of velocity (3.22). Substitution of the result into (3.23) reduces the equation expressing the continuity of the velocity gradient to a quadratic in d. Again, only one root is physically relevant (i.e., real and positive). The results for a given volume are again selected from the complete set of results.

d. Computational techniques

A set of programs, written in the language C to run on a Macintosh Plus computer, have been developed to evaluate the above analytic solutions. The programs allow for the computation and display of interface and velocity profiles for a wide variety of rings. As a check on the computations, the solution within Region II is computed in two different ways. In addition to a straightforward evaluation of the analytic solution derived above, an additional calculation is made using a fourth-order Runge-Kutta method to integrate the velocity field equations directly. To the accuracy of computations, both methods agree.

5. Results

a. Typical interface and velocity profiles

Following typical measurements of warm-core ring 82B (Schmitt and Olson, 1985) the initial conditions for the system, prior to cooling, were chosen to be

TABLE 1. Initial conditions.

	Temperature (°C)	Salinity (‰)	Density kg m^{-3}
Initial condition of ring	18	36.5	1026.43
Mixed layer	13	35.5	1026.78
Lower layer	5	35.0	1027.68
Undisturbed mixed-layer depth	50 m		
Ring volume	2.13×10^{12} m^3		

These parameters are meant to be representative of a newly formed warm-core ring and will serve to illustrate the processes involved. Calculations for other initial conditions show only quantitative differences in the process. With these parameters, the initial value of the density defect ratio, d, is -0.41, the outer radius of deformation, R_d, is $\sim$6.5 km, and the initial ring radius is 56 km.

The mixed-layer is meant to represent a single thin layer of the surrounding fluids and not necessarily the classic oceanographic mixed layer which arises at the surface. In general, the fluids surrounding a ring will be stratified and the overflooding mechanism is expected to apply to each individual "layer" in the stratified fluid. Thus, we are interested in looking at the overwashing of individual thin layers.

A ring volume of 2.13×10^{12} m^3 was chosen because it corresponds to a nondimensional ring volume of 1000. The heat flux is taken to be illustrative of what can occur in the ocean. Schmitt and Olson (1985) report heat fluxes on the order of 2000 W m^{-2} during winter storms. If this level of cooling were applied for several days, followed by a similar period of no cooling (to allow adjustment time for any transients), the net cooling would be equivalent to a continuous cooling at 1000 W m^{-2}, the value used in this paper to provide some form of a time reference. While the actual heat flux may vary dramatically over the time scales of days, this heat flux will serve as basis for examining the effects of cooling.

An entire series of profiles were generated from these initial conditions showing the ring in cross section as it sank. Four of these profiles, plotted on nondimensional scales, are shown in Fig. 6. In these plots, a unit distance corresponds to 50 m in the vertical and $\sim$6.5 km in the horizontal. The profile of the ring under its initial conditions is shown in Fig. 6a. The ring at this point is about 112 km in diameter. The initial injection of the ring has compressed the mixed layer, forcing some mixed-layer fluid to flow outward, thus anticyclonically spinning up the mixed layer.

Figure 6b is the profile for the same ring cooled to 16.6°C. At this point the density defect ratio has been reduced to -0.04. As a point of reference, this drop in ring temperature would be equivalent to a continuous cooling of 1000 W m^{-2} for a period of just over 15 days. The denser ring has sunk in the middle, further compressing the mixed layer below the ring. The interface between the ring and the mixed layer is steepening.

Cooling the ring an additional 0.1°C would result in the ring having the same density as the mixed layer. As pointed out previously, this point cannot be computed by the model (because $\epsilon \rightarrow \frac{1}{2}$), but the form of the interface at this point can be described. When $d = 0$, the mixed layer below the ring will have zero thickness so all of the mixed-layer fluid will have been displaced to outside of the ring. The mixed-layer fluid adjacent to the ring will be accelerated to the velocity of the ring. The interface between the ring and the mixed layer will be vertical as there will be no density or velocity difference across the interface. Noting that the system will in general spend very little time in this state, it is doubtful that the system would exhibit any singular behavior at this point.

Figure 6c shows the profiles of the ring soon after sinking ($d = 0.0031$). The ring has been completely overwashed by the mixed-layer fluids, but note that the overwashing layer is extremely shallow (on the order of 5 cm) in the central portions of the ring. After this overwashing occurs, the source of differential cooling disappears. Still, there are at least two reasons why it is instructive to consider what would happen if the ring would continue to cool past this point. First, it can be shown that the effects of continued ring cooling are the same as those resulting from a warming of the surrounding fluids (section 5c), a situation which occurs in the late-spring and summer. Second, even in the case of continued surface cooling, we can speculate that the thin overwashing layer will be quickly mixed into the ring allowing the ring to continue its cooling. It should be noted though that the model does not strictly apply to the latter situation due to the introduction of new fluid into the ring.

In this spirit, Fig. 6d shows the ring as if it had been cooled to 15.4°C. This again corresponds to a continuous cooling at a mean rate of 1000 W m^{-2} for a period of about 16 days. The ring has continued to deepen during this period and its diameter has been reduced to 94 km. The mixed layer over the ring has also deepened to a depth of several meters in the center of the ring.

Figure 7 shows the nondimensional mixed-layer azimuthal velocity profiles for the same four cases as shown in the interface profiles. Note that the velocity in the mixed layer increases as the ring approaches the density of the mixed layer and then subsides as the ring density increases beyond that of the mixed layer. In the limits where d approaches zero, the mixed-layer velocity approaches the velocity of the ring, $-r/2$. When $d = 0$ (not shown) the mixed-layer is pushed outside of the ring and the velocity discontinuity between the

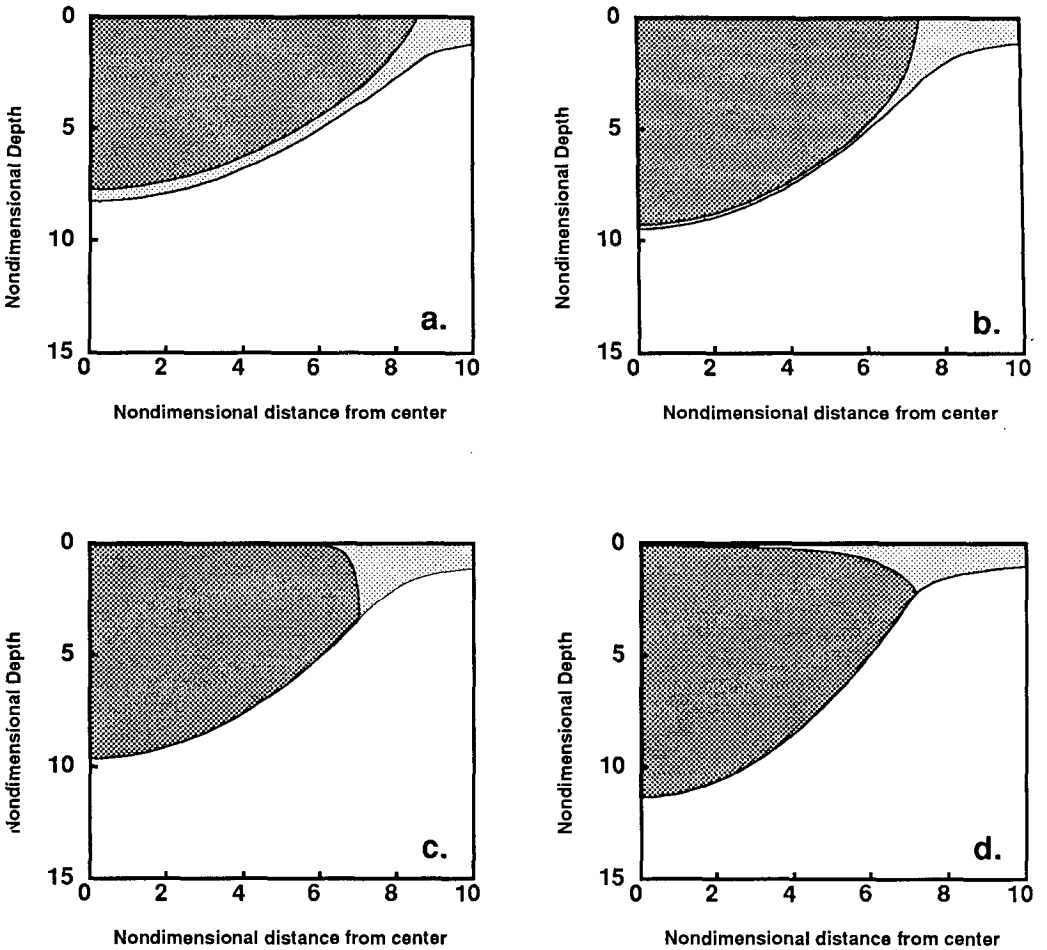

FIG. 6. Interface profiles for a sinking warm-core ring: (a) the initial state of the ring with temperature 18.0°C (other initial conditions are given in Table 1), (b) after cooling the ring to 16.6°C (equivalent 1000 W m^{-2} continuous cooling for a period of just over 15 days), the ring is nearly ready to sink below the mixed layer. The sinking ring has displaced most of the mixed layer spinning up the mixed-layer fluid as it is forced outside of the ring. Cooling the ring to 16.5°C causes the ring to submerge (c). During the submergence, the mixed-layer fluid overfloods the ring completely, although the overflooding layer is very shallow in the center of the ring. Finally in (d) the ring has continued to cool to 15.4°C. The mixed layer continues to flood over the ring as the ring continues to sink into the passive lower layer.

ring and the mixed layer disappears. In this case the mixed layer reaches a maximum dimensional velocity of just over 1 m s^{-1}.

b. Parcel trajectories

In addition to interface and velocity profiles, the trajectories of individual fluid parcels can be tracked. (Here, it is assumed that one can average over a number of weak cooling events to obtain a continuous description.) The azimuthal motion of individual fluid parcels is given by an integration of the azimuthal velocity, and their radial motion can be tracked through the application of angular momentum conservation. Prior to the initial injection of the ring, each parcel of fluid in the mixed-layer has an angular momentum which uniquely depends upon the parcel's radial position. Since the angular momentum of each parcel is invariant, the initial angular momentum can be used as a tag for each parcel. It is important to realize that, in our model, the level of the free surface at the center ($r = 0$) remains fixed at all times. The ring sinks relative to the fluid in which it is embedded.

The general motion of the mixed layer as a surfaced ring sinks is an anticyclonic, outward and generally upward spiral pattern. When the ring submerges and continues to sink, the mixed layer trajectories form anticyclonic, inward spiral patterns. The overall paths of the mixed-layer parcels resembles a vertical helical spring that is narrow at the ends and thick in the middle. An example of this parcel motion is shown in Fig. 8.

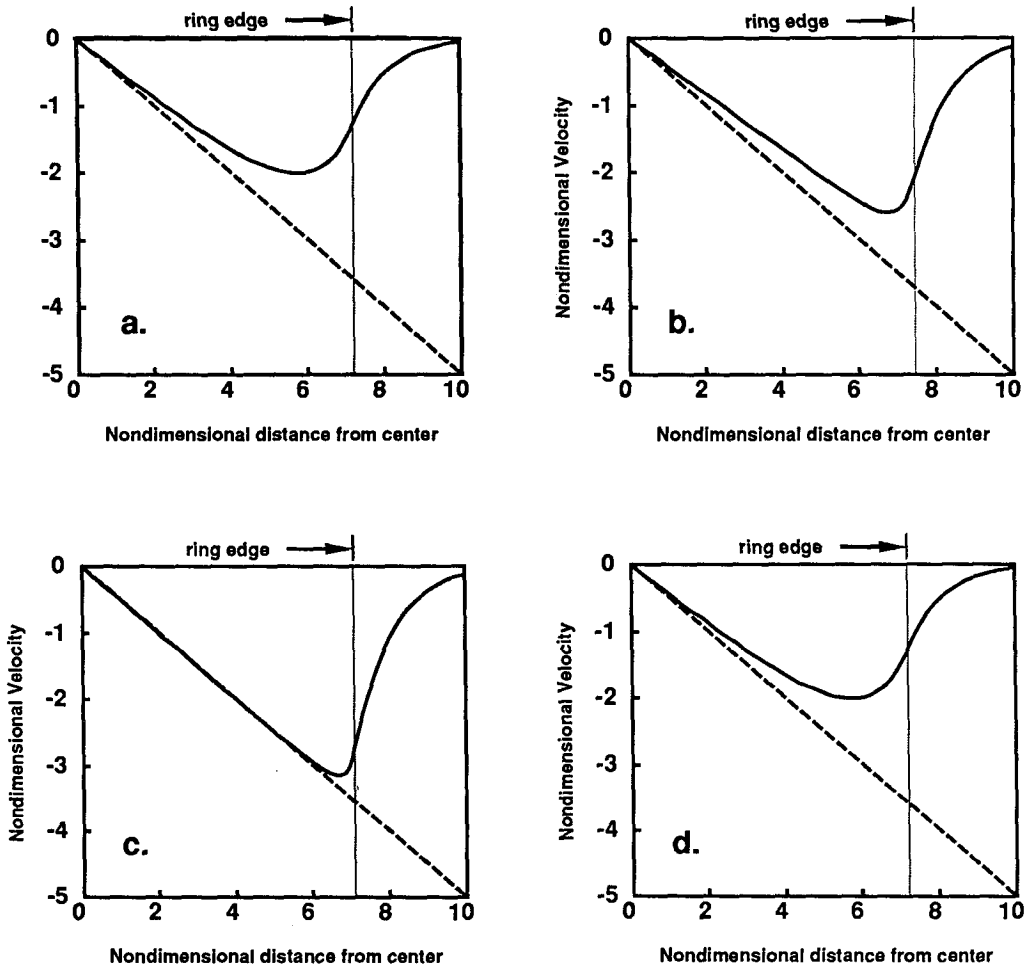

FIG. 7. Azimuthal velocity profiles for the mixed layer (solid line) and ring (dashed line) for the same four conditions shown previously (Fig. 6). The ring, being modeled as having zero-potential vorticity, is always in solid body rotation with nondimensional velocity $-r/2$. The mixed layer is spun up as the ring approaches the point of submergence (a-b) and then spun back down as the ring submerges and the mixed layer overfloods the ring (c-d).

Figures 9a and 9b show the trajectory of a single parcel (as seen from above) corresponding to the ring shown in Figure 6). Figure 9a shows the outward spiral form of the parcel that starts below the ring. Figure 9b shows the inward spiral form of the same parcel as the ring sinks. Note that other particles behave in a very similar fashion. The grey areas show the initial area of the ring (which shrinks somewhat as the ring sinks). The plotted parcel was initially (i.e., prior to the injection of the ring) two deformation radii from the center. These spirals do not appear to progress to the outside of the ring due to the model's breakdown near the point of equal ring and mixed layer densities. In fact, all of the fluid parcels in the mixed layer are forced outside of the ring when $d = 0$.

There are two major points to be made regarding these trajectory results. First, the model predicts that the initial fluid that overwashes a ring originates from *under the ring and not from outside of the ring.* Once the volume of the overwashing fluid equals the initial volume of underlying fluid, any continued cooling will begin to pump outside fluid into the ring. Second, the overwashing fluid spirals in from all directions due to the symmetry of the model.

This model is unable to explain the typically asymmetric appearance of streamers. Conceptually, asymmetries could be introduced into the overwashing fluids in several ways. First, a portion of the underlying fluids could be marked by an essentially passive tracer. This tracer would then be visible as the fluids overwash the ring. Second, the underlying fluids could be dynamically asymmetric due to their being embedded in a flow or the presence of a front under the ring. It is not difficult to imagine how a horizontal temperature gradient in the overwashing fluids could lead to a visible spiral structure. A third alternative is that the asym-

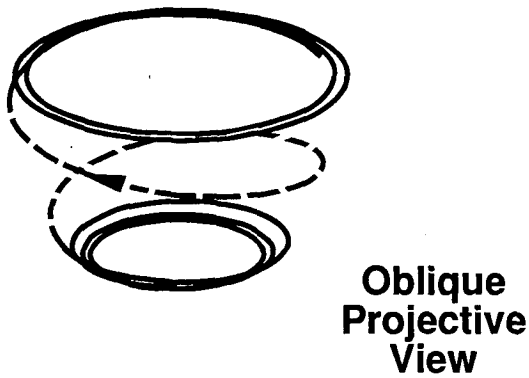

FIG. 8. A three-dimensional view of the trajectory of a selected mixed-layer parcel during ring submergence. As the ring sinks, the mixed layer parcels are displaced outward and upward, all the time with a general anticyclonic motion. The ring then sinks and the mixed layer parcels spin up and overfloods the ring. This particular path represents a similar period of cooling as that discussed in Fig. 6. This figure is taken from the model, but a period in the center of the trajectory, when the ring has nearly the same density as the mixed layer, had to be interpolated since the model breaks down in this region (dashed line).

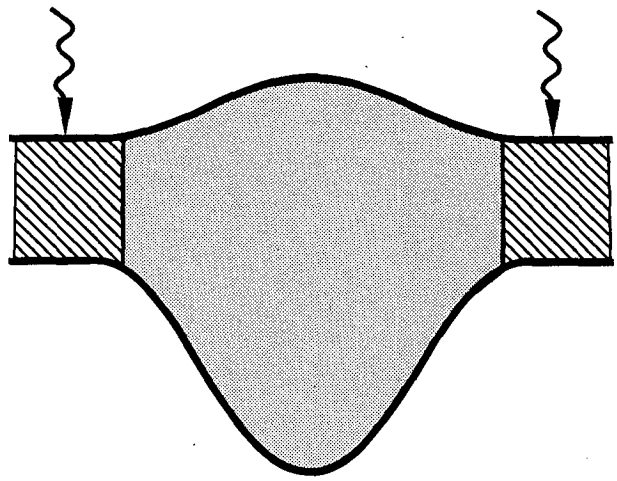

FIG. 10. A sketch of the initial conditions for applying the model to the process of differential atmospheric warming. In this beginning state, the ring and mixed-layer densities are assumed to be equal.

metry is due to some instability in the overwashing fluids that tends to concentrate the overwashing event into a single spiral band. It is impossible to say with the current model which, if any, of these mechanisms is important for the production of streamers.

c. *Vernal warming*

The model has been described so far in terms of the differential cooling of the ring relative to the surrounding fluids. Anyone still reading at this point may well wonder about the obvious alternative mechanism, a warming of the surrounding fluids relative to the ring. It seems obvious that the differential warming of surrounding fluids could also lead to overflooding of the ring. Differential warming can be expected to occur during late spring when the atmosphere begins to warm, but the ring is still warmer at the surface than the surrounding shelf water.

It can be shown that when the densities of the ring and mixed layer are initially equal, then the effects of

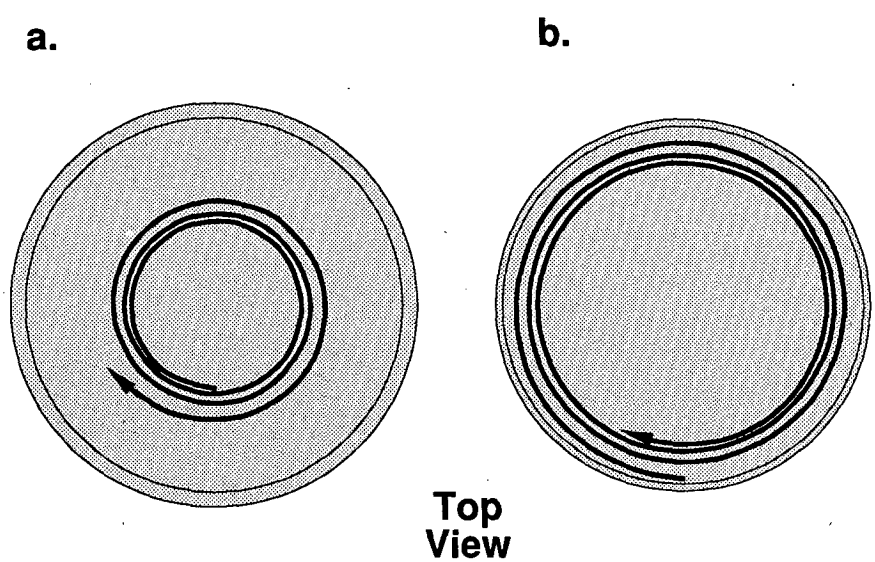

FIG. 9. An overhead view of the parcel as it spirals outward from underneath the ring is shown in (a). The concentric circles represent the initial ring edge (outer circle) and the edge of the ring just prior to sinking (inner circle). A similar view of the parcel overflooding and spiralling into the ring is given in (b). Each of the figures represents a drop in ring temperature of about 1.2°C. The parcel shown in this figure is the same parcel as depicted in Fig. 8. Prior to the injection of the ring this parcel was initially two deformation radii from the center.

differential atmospheric warming of the mixed layer can be modeled using the same analysis as for the cooling of a ring. (A sketch of the required initial condition is shown in Fig. 10.) Note that the initial condition of equal ring and mixed-layer densities may be arrived at through a period of active cooling just prior to the warming episode, a situation which is similar to what occurred in ring 82B. In this case, the only difference between the analyses for warming and cooling is the depth of the layer being subjected to the heat flux. In general, the mixed layer will be warmed faster than the ring is cooled for the same magnitude of surface heat flux. An example parcel trajectory over a 5-day period of 1000 W m^{-2} mixed layer warming is shown in Fig. 11. (Although one might expect the differential heat fluxes to be lower than this value in the case of vernal warming, this value was chosen to be consistent with the previous analysis.) The spiral angle is steeper than those obtained for the case of the ring cooling due to the smaller heat capacity of the mixed layer.

d. Comparison with 82B data

Available meteorological data shows that ring 82B had been subjected to substantial cooling from its inception in February until sometime in late April or early May. The effects of the cooling are evident in the steepening of the 10°C isotherm that was observed to occur from March to April. Figure 12 shows the radial distribution of the 10°C isotherms as derived from XBT surveys during March and April [reproduced from Olson et al. (1985)]. The profiles produced by this model show the same type of steepening of the isotherms as displayed in Fig. 12.

Figure 13 shows the potential temperature cross section of ring 82B in April (Schmitt and Olson, 1985).

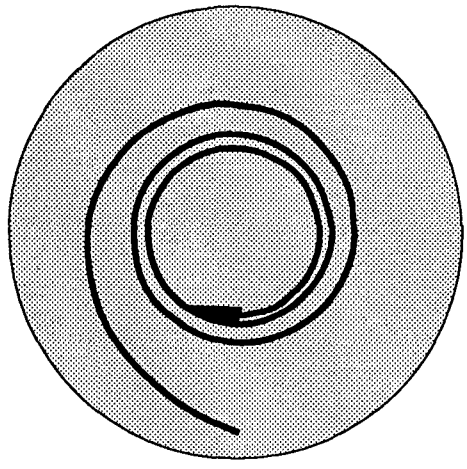

FIG. 11. A view of a mixed-layer parcel overflooding and spiralling into the ring for the case of mixed-layer warming. The spiral angle is steeper here than in Fig. 9 since the thin mixed layer changes density faster than the thicker ring for same magnitude of the surface heat flux.

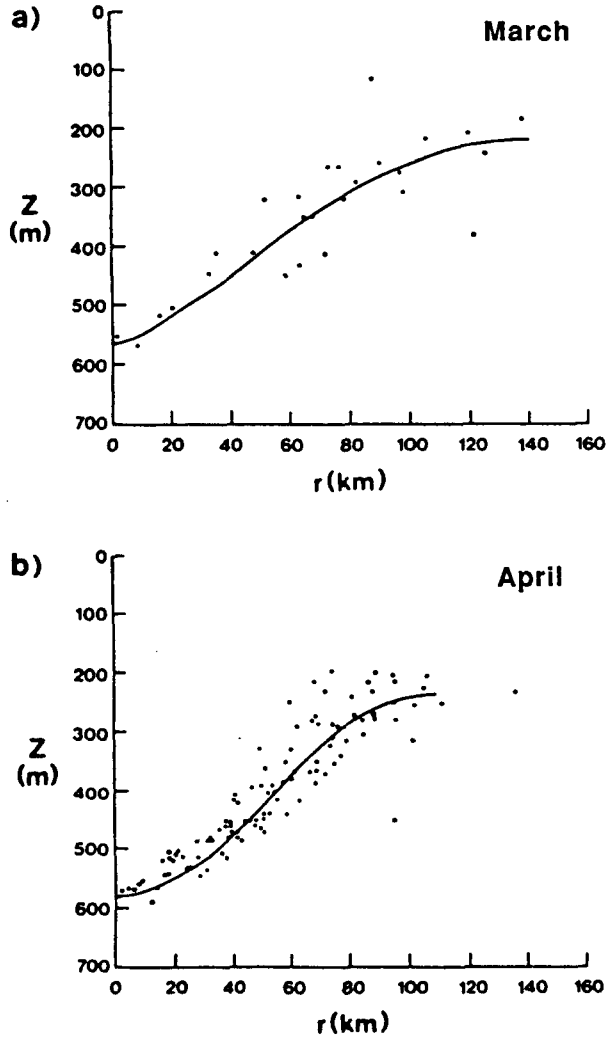

FIG. 12. The radial distribution of 10°C isotherms from warm-core ring 82B in March (a) and April (b), a period of substantial cooling over the ring. The general steepening of the isotherms appears to be forced by the sinking of the ring in the surrounding fluids, just as in the model.

The profiles, with the characteristic steep ring edge interface, appear similar to those for a ring that is about to sink. In fact, there is a hint of overflooding occurring in this profile in the form of surface cooling at the edge of the ring. A satellite image from this same period (Fig. 14, see p. 566) shows thin, wispy tendrils of cooler shelf water apparently spiraling into the ring from all directions around the center. As pointed out by an anonymous reviewer, the asymmetries of this inflow could also be caused by instabilities in the interface between the ring and the mixed layer, but this is not necessarily inconsistent with the mechanism we propose here.

Streamers of cold shelf water were not observed to spiral in towards the center of 82B until the vernal warming began in May. Figure 1 shows the typical spi-

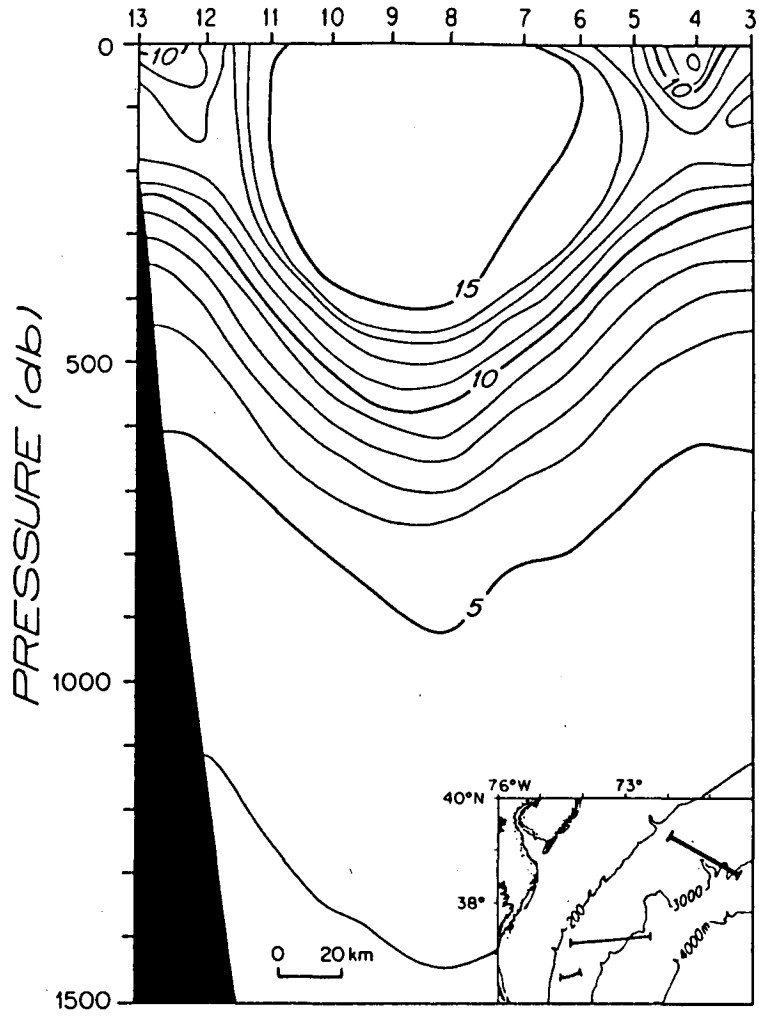

FIG. 13. Potential temperature cross-section of ring 82B in April. The ring isotherms are very steep indicating that the ring is of nearly the same density as the surrounding fluids. A hint of active overflooding can be seen from the impingement of the cooler surrounding waters overtop the ring's edge.

ral pattern associated with the inflow of the surrounding surface waters. In the case of 82B, we believe that these streamers are due, at least in part, to the differential warming of the surrounding fluids.

6. Discussion

a. Modeling assumptions

As in nearly all analytical models, simplifications have been made to make the problem tractable. The major question here is whether the model has been oversimplified to the point where the results are not applicable or are even misleading. The following simplifications are thought to be critical.

As in Gill (1981), the ring formation process described here involves the injection of the ring material into a previously resting ocean. This formation process was chosen as the only way to obtain a uniform potential vorticity in the mixed layer while maintaining finite velocities at infinity. In order to get a better idea of the efficacy of this assumption, consider an alternative initial condition. Suppose that the initial condition was a surfaced zero-potential vorticity ring which was surrounded by a resting mixed layer (Fig. 15). Clearly, this implies a nonuniform potential vorticity throughout the mixed layer because the mixed layer depth varies near the ring. It also implies a large shear between the ring and the surrounding fluids. If the ring is cooled and sinks, or the outer fluid is warmed, the surrounding fluids will again overwash the ring. This time though, as the fluid parcels move inward over the ring they will be spun up cyclonically. To our knowledge, cyclonic flows are not observed on top of rings. (Although small cyclonic ringlets on the periphery of warm-core rings have been described by Kennelly et

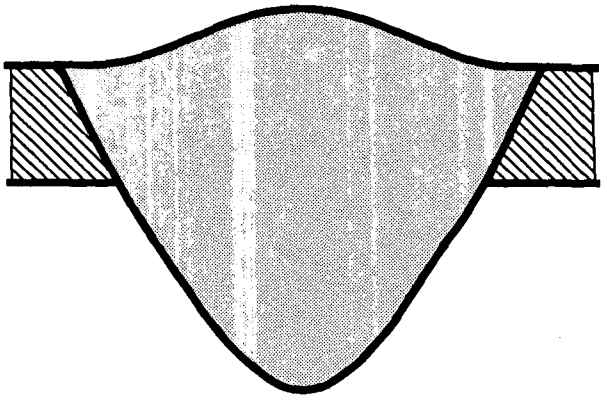

FIG. 15. An alternative initial condition consisting of a surfaced zero-potential vorticity ring surrounded by a resting mixed layer. Note that this implies a nonuniform potential vorticity throughout the mixed layer because the mixed layer depth varies near the ring.

al. (1985), these are not of significance for this argument.) The actual flows surrounding warm-core rings are probably somewhere between these two extremes of no spin up and a "complete" spin up of the outer fluid. Still, it is believed that the model presented does capture the essence of what occurs during a sinking event.

As in Nof (1983) and Adamec and Elsberry (1985), a very special form of cooling (or warming) has been used within the model in order to maintain the conservation of potential vorticity (Fig. 3). It is safe to say that a heat flux of exactly this type will never be observed. Still there is good reason to expect the heat flux to be tapered. In general, the heat flux is predominantly determined by the air–sea temperature difference. The ring, having a higher surface temperature than the surrounding fluids, can be expected to lose heat to a cold atmosphere faster than the surrounding cold fluids. Furthermore, differential cooling may occur within the ring if the surface temperature of the ring decreases horizontally away from ring center. Similar arguments can be made for the situation of a positive heat flux into the ocean from a warm atmosphere.

The model has the simplest possible characterization of stratification. Conceptually, the fully stratified case can be thought of as a succession of thin layers, each behaving in much the same manner as the single thin layer in this study. Gill (1981) examined the intrusion of fluid into an infinite stratified ocean, though the lack of a free-surface in Gill's model precludes its applicability to warm-core rings.

The ring itself was modeled as having zero potential vorticity. This can be viewed as a limiting case for rings since this produces a ring with maximum steepness and nonlinearity. Kunze (1986) measured a relative vorticity $[(1/r)d(rV_\theta)/dr]$ of $-f/2$ in warm-core ring 82I, only a factor of two less than that required for zero potential vorticity. Several effects occur if slower rings are considered. Slower rings are more shallow, thus they displace less mixed-layer fluid than faster rings of the same density and volume. This implies that the overwashing fluids will tend to spin slower for a slow ring than for a fast ring. At the same time the surface area of slower rings is increased, increasing the rate of cooling. Both of these effects combine to increase the angle of the overwashing spiral. Thus, it is expected that the spiral angles occurring in real warm-core rings, which have lower potential vorticity than the ring modeled here, may be steeper than the curves shown here for the case of ring cooling.

b. Implications for biological productivity

The biology of warm-core rings has been the focus of several studies. It was originally thought that warm-core rings were biologically unproductive, since they originate in relatively unproductive waters. It is now known that significant growth of the biota in a warm-core ring can occur, making the ring even more productive than the surrounding waters. Studies by Tranter et al. (1982, 1983) suggest that upwelling near the edges of rings is the principal mechanism causing the enhanced biological production. Franks et al. (1986) suggests that frictional decay causes the ring to flatten out thus pumping nutrient-rich waters from the depths of the ring into the euphotic zone.

The reports by Smith and Baker (1985), Davis and Wiebe (1985), Wiebe et al. (1985), and Olson (1986) suggest a much more complex picture, at least for ring 82B. Initially the ring was well mixed and nutrient rich, but low in productivity due to the mixing of phytoplankton below the euphotic zone. Then in May, vernal warming capped the ring, stopping the convective overturn within the ring. This was followed by successive blooms of phytoplankton and zooplankton. Davis and Wiebe (1985) report that the bloom in macrozooplankton was dominated by shelf water species that were probably introduced into the ring through the lateral exchange associated with streamers.

Our model suggests that such a lateral exchanges may be due to differential cooling or warming events that are sufficiently strong to bring in fluids from outside of the ring. Furthermore, the model shows how layers that originate below a ring can be brought to the surface over the top of the ring. These layers, having been trapped below the ring since its creation, may be richer in nutrients than the surface waters in the ring, thus causing an increase in biomass production.

c. Additional comments

Observations of ring 82B appear to be consistent with the results of this model. The model suggests a possible mechanism for the formation of streamers. The cooling model is incomplete because it assumes that the mixed layer overwashes the ring without being cooled itself. In reality, it is expected that the mixed

layer would be cooled and then mixed into the ring as it overwashes the ring. This is exactly what appears to have happened in ring 82B. The satellite imagery of 82B during the period of cooling does not show visible entrainment of fluid into the center of the ring, but instead shows the spiral inflow of fluid at the ring edge and well mixed ring center (Fig. 14).

Streamers were observed though in 82B after the cooling stopped in May and the vernal warming began (e.g. Fig. 1). In this situation, it seems possible that the visible overwashing of fluid associated with a streamer became possible only after the cooling was turned off. The convective mixing associated with cooling would tend to mix out any visible surface signature of the inflow and this may be what happened in 82B. Thus, we attribute the initial formation of streamers in 82B to differential vernal warming of the surrounding fluids.

7. Summary

The simplest possible analytic model of the sinking of warm-core rings has been presented. The model examines the dynamics of a zero-potential vorticity ring being cooled in an otherwise two-layer ocean. Similar behavior is expected when, instead of cooling the ring, the environmental fluid is being warmed. The results show that as the ring becomes denser, it displaces the mixed layer under it (Figs. 6a and 6b), spinning up the mixed layer anticyclonically in the process (Figs. 7a and 7b). As the ring becomes denser than the surrounding fluids, it sinks and is completely overwashed. In the case of cooling, this overwashing layer is thin in the central portions of the ring when the model breaks down. In the case of warming, however, the model never breaks down and the ring continues to sink [shrinking in surface area as it increases in depth (Figs. 6c and 6d)] as long as the warming continues. The overwashing fluid continues to spiral in over the ring, spinning down as the ring continues to sink (Figs. 7c and 7d). Overall, mixed-layer parcels follow an upward helical motion as pictured in Fig. 8. It is speculated that the spiral form of mixed-layer fluid parcel trajectories can lead to the formation of streamers, although why streamers are manifested by a single spiral arm of fluid is not known.

Comparisons with data from ring 82B suggest that spiral inflow of surface waters did occur in 82B during April 1982. This inflow was initially mixed into the ring thermostad through convective overturning and so there was little apparent surface signature marking the inflow. The first visible streamers appeared soon after the cooling stopped and vernal warming began, the cessation of overturning allowing the inflow to become visible.

The model presented here has several implications regarding the enhanced biological growth observed in rings. The model provides a dynamic mechanism for the observed introduction of shelf-water species into the ring interior. These opportunistic interlopers are then ready to take advantage of the nutrient rich surface waters of the ring when vernal warming finally caps the ring and brings about the spring blooms. The model also suggests a mechanism for the introduction of nutrients into the ring.

Acknowledgments. We wish to thank D. Olson for useful discussions regarding the comparison of the model to observations and for providing the satellite images. William Dewar made many useful suggestions regarding the theoretical development of the model; Lou Howard provided insights into the associated adjustment processes. We'd also like to thank Steve VanGorder who carefully checked all of the computations. During the course of this work, R. Chapman was supported by a NASA Remote Sensing Traineeship, a Florida State University Graduate Fellowship, and ONR (N00014-82-C-0404). D. Nof was supported by ONR (N00014-82-C-0404) and NSF(1368-586-22).

APPENDIX A

Region I Cannot Exist in the Surfaced Ring Case

This appendix contains a proof that Region I (Fig. 4) cannot exist; that is, there can be no intersection point between the ring-mixed layer interface and the mixed layer-lower layer interface. We proceed by *abductio ad absurdum.* First assume that such an intersection exists, implying $\xi_M(r_1) = \xi_{RI}(r_1)$ for some r_1 between 0 and r_0. Applying the solutions for the interface displacements in terms of the velocity [(3.11c) and (3.11d)] provides the condition for intersection

$$\frac{\vartheta_M(\alpha_1)}{\alpha_1} + \frac{\partial \vartheta_M}{\partial \alpha}(\alpha_1) = 0 \tag{A1}$$

where, as before, $\alpha_1 = r_1/r_0$.

Leaving this information aside for the moment, note that the mixed-layer thickness goes to zero at the intersection. This, combined with the conservation of potential vorticity, implies that the velocity of the mixed-layer fluid at the intercept point is $V_{\theta M}(r_1) = -r_1/2$, which is equivalent to $\vartheta_M(\alpha_1) = 0$. Thus (A1) implies that $(\partial \vartheta_M/\partial \alpha)_{\alpha=\alpha_1} = 0$. Finally apply both of these conditions on ϑ_M to the velocity field equation in region II (3.11a),

$$\frac{\partial^2 \vartheta_M}{\partial \alpha^2}(\alpha_1) = \frac{(1-d) r_0^4 \alpha_1}{4d} < 0 \tag{A2}$$

since $d < 0$. Further note that ϑ_M and its first and second derivatives are continuous [because of (3.12)]. Here, a Taylor series expansion shows that there exists a finite δ such that $\vartheta_M(\alpha_1 + \delta) < 0$. This implies that

$$V_{\theta M}(r_1 + \delta r_0) < -(r_1 + \delta r_0)/2 \tag{A3}$$

but, as will be shortly shown, this is impossible.

Each and every mixed layer parcel must have originated at some point $r_i > 0$ prior to the injection of the ring. This together with the conservation of angular momentum, implies that the *minimum* velocity obtainable by any mixed layer parcel is $-r/2$, so that the minimum velocity obtainable by a mixed layer parcel at $(r_1 + \delta r_0)$ is $-(r_1 + \delta r_0)/2$. Hence there is a contradiction between the velocity restriction derived from the conservation of angular momentum and (A3). Thus the assumption of an intersection point must be false.

APPENDIX B

Region I Cannot Exist in the Submerged Ring Case

As before, assume that there does exist a single point r_1 where the ring intersects the surface (Fig. 5). By the same angular momentum argument as before, the nondimensional velocity of the mixed layer parcel at this point must be $-r_1/2$, which is equivalent to $\vartheta_M(\alpha_1) = 0$.

Again the condition for intersection is given by (A1) which implies that $(\partial\vartheta_M/\partial\alpha)_{\alpha=\alpha_1} = 0$. Note that the field equation in ϑ_M, (4.7), is second order and homogeneous, so if ϑ_M and its first derivative are zero at a regular point and ϑ_M is analytic at that point then ϑ_M is zero everywhere in Region II. This is a result of the fact that the second derivative and all higher derivatives are also zero so that a Taylor series expansion will give zero velocity everywhere. Hence, in Region II, the nondimensional velocity in the mixed layer is $-r/2$ *everywhere* so that the surface and upper ring interface are *parallel* and must intersect everywhere.

REFERENCES

Adamec, D., and R. L. Elsberry, 1985: Response of an intense oceanic current system to cross-stream cooling events. *J. Phys. Oceanogr.*, **15,** 273–287.

Chapman, R. D., 1987: The cooling and sinking of warm-core rings, Ph.D. dissertation, Florida State University, 68–73.

Davis, C. S., and P. H. Wiebe, 1985: Macrozooplankton biomass in a warm-core ring: time series changes in size structure, taxonomic composition, and vertical distribution. *J. Geophys. Res.*, **90,** 8871–8884.

Dewar, W. K., 1987: Ventilating warm rings: Theory and energetics. *J. Phys. Oceanogr.*, **17,** 2219–2231.

——, and G. R. Flierl, 1985: Particle trajectories and simple models of transport in coherent vorticies. *Dyn. Atmos. Oceans,* **9,** 215–252.

Evans, R. H., K. S. Baker, O. B. Brown and R. C. Smith, 1985: Chronology of warm-core ring 82B. *J. Geophys. Res.*, **90,** 8803–8811.

Flierl, G. R., 1979: A simple model for the structure of warm and cold core rings. *J. Geophys. Res.*, **84,** 781–785.

——, and R. P. Mied, 1985: Frictionally induced circulations and spin down of a warm core ring. *J. Geophys. Res.*, **90,** 8917–8927.

Franks, P. J. S., J. S. Wroblewski and G. R. Flierl, 1986: Prediction of phytoplankton growth in response to the frictional decay of a warm-core ring. *J. Geophys. Res.*, **91,** 7603–7610.

Gill, A. E., 1981: Homogeneous intrusions in a rotating stratified fluid. *J. Fluid Mech.*, **103,** 275–295.

Ikeda, M., 1982: A simple model of subsurface mesoscale eddies. *J. Geophys. Res.*, **87,** 7925–7931.

Joyce, T. M., and M. Stalcup, 1985: Wintertime convection in a Gulf Stream warm-core ring. *J. Phys. Oceanogr.*, **15,** 1032–1042.

Kennelly, M. A., R. H. Evans and T. M. Joyce, 1985: Small-scale cyclones on the periphery of a Gulf-Stream warm-core ring. *J. Geophys. Res.*, **90,** 8845–8858.

Killworth, P. D., 1983: On the motion of isolated lenses on a beta-plane. *J. Phys. Oceanogr.*, **13,** 368–376.

Kunze, E., 1986: The mean and near-inertial velocity fields in a warm-core ring. *J. Phys. Oceanogr.*, **16,** 1444–1461.

Nof, D., 1981: On the β-induced movement of isolated baroclinic eddies. *J. Phys. Oceanogr.*, **11,** 1662–1672.

——, 1983: On the response of ocean currents to atmospheric cooling. *Tellus,* **35A,** 60–72.

Olson, D. B., 1986: Lateral exchange within Gulf Stream warm-core ring surface layers. *Deep-Sea Res.*, **33,** 1691–1704.

——, R. W. Schmitt, M. A. Kennelly and T. M. Joyce, 1985: A two-layer diagnostic model of the long-term physical evolution of warm-core ring 82B. *J. Geophys. Res.*, **90,** 8813–8822.

Schmitt, R. W., and D. B. Olson, 1985: Wintertime convection in warm-core rings: thermocline ventilation and the formation of mesoscale lenses. *J. Geophys. Res.*, **90,** 8823–8844.

Shay, T. J., and M. C. Gregg, 1986: Convectively driven turbulent mixing in the upper ocean. *J. Phys. Oceanogr.*, **16,** 1777–1798.

Smith, R. C., and K. S. Baker, 1985: Spatial and temporal patterns in pigment biomass in Gulf Stream warm-core ring 82B and its environs. *J. Geophys. Res.*, **90,** 8859–8870.

Stommel, H., and G. Veronis, 1980: Barotropic response to cooling. *J. Geophys. Res.*, **85,** 6661–6666.

Tranter, D. J., G. S. Leach and D. J. Vaundrey, 1982: Biological significance of surface flooding in warm-core eddies. *Nature,* **293,** 751–755.

——, —— and D. Airey, 1983: Edge enrichment in an ocean eddy. *Aust. J. Mar. Freshw. Res.*, **34,** 665–680.

Veronis, G., 1956: Partition of energy between geostrophic and non-geostrophic oceanic motions. *Deep Sea Res.*, **3,** 157–177.

Wiebe, P. H., G. R. Flierl, C. S. Davis, V. Barber and S. H. Boyd, 1985: Macrozooplankton biomass in a warm-core ring: spatial distribution and temporal changes. *J. Geophys. Res.*, **90,** 8885–8901.